Nuclear Instruments and Methods in Physics Research A 643 (2011) 57–63

Contents lists available at ScienceDirect

Nuclear Instruments and Methods in Physics Research A

journal homepage: www.elsevier.com/locate/nima

The development and performance of UV-enhanced APD-arrays for high resolution PET imaging coupled with pixelized Pr:LuAG crystal

M. Yoshino [a,*], J. Kataoka [a], T. Nakamori [a], H. Matsuda [a], T. Miura [a], T. Katou [a], Y. Ishikawa [b], N. Kawabata [b], Y. Matsunaga [b], K. Kamada [c], Y. Usuki [c], A. Yoshikawa [d], T. Yanagida [d]

[a] Research Institute for Science and Engineering, Waseda University, 3-4-1, Ohkubo, Shinjuku, Tokyo, Japan
[b] Solid State Division, Hamamatsu Photonics K. K., 1126-1, Ichino-cho, Hamamatsu, Shizuoka, Japan
[c] Materials Research Laboratory, Furukawa Co., Ltd., 1-25-13, Kannondai, Tsukuba, Ibaraki 305-0856, Japan
[d] IMRAM, Tohoku University, 2-1-1 Katahira Aoba-ku, 980-8577 Sendai, Japan

ARTICLE INFO

Article history:
Received 29 September 2010
Received in revised form
2 March 2011
Accepted 22 March 2011
Available online 30 March 2011

Keywords:
Avalanche photodiode
Gamma-rays
Positron emission tomography

ABSTRACT

The development of high-resolution, UV-enhanced avalanche photodiode (APD) arrays usable in high-resolution PET imaging is underway. These APD arrays were specifically designed as photosensors capable of direct coupling with pixelized Pr-doped $Lu_3Al_5O_{12}$ (Pr:LuAG) scintillators. An excellent quantum efficiency (QE) of 55% was achieved at the peak emission of Pr:LuAG (310 nm), namely, a substantial improvement from the QE $\lesssim 5\%$ as measured with the conventional Hamamatsu reverse-type APDs (S8664 series). Each APD device has 8×8 (TYP1) and 12×12 (TYP2) pixel structures with active areas of 3×3 mm^2 and 2×2 mm^2 in each pixel, respectively. A gain uniformity of $\pm 8\%$ and low dark noise of $\lesssim 2$ nA/pixel have been achieved, measured at $+25$ °C. We also report on the large size single crystal growth of improved Pr:LuAG scintillators and the preliminary performance test of the same. An energy resolution of 4.2% (FWHM) was obtained for 662 keV gamma-rays for $10\times 10\times 10$ mm^3 crystal, measured with a PMT employing a super-bialkali photocathode. We made a test module consisting of a UV-enhanced APD-array (either TYP1 or TYP2) optically coupled with an 8×8 (or 12×12) pixel Pr:LuAG matrix. The linearity between the output signals and incident gamma-ray energy of TYP1 and TYP2 gamma-ray detectors were only 0.27 and 0.33%, as measured at $+25$ °C for various gamma-ray sources, respectively. Energy resolutions of $7.0\pm 0.2\%$ (FWHM) and $9.0\pm 0.6\%$ (FWHM) were, respectively, obtained for TYP1 and TYP2 detector arrays for 662 keV gamma-rays. The uniformity of the pulse height distributions was also measured at less than 8% for both detectors. Finally, we measured the coincidence timing resolution of these gamma-ray detectors and obtained 4.0 ± 0.1 ns (FWHM) for the 511 keV annihilation quanta from a ^{22}Na source. These results suggest that UV-enhanced APD-arrays coupled with Pr:LuAG scintillators could be a promising device for future application in nuclear medicine.

1. Introduction

The avalanche photodiode (APD) is a compact, high-performance light-sensor recently applied in various fields of experimental physics. In particular, the reverse-type APD offers significant advantages in detecting weak light scintillation signals, thanks to its narrow high-field amplification region close to the front end [1–3]. A high quantum efficiency (QE) of $\gtrsim 80\%$ is achieved over the wavelength range of 500–830 nm. Moreover, this type of APD works at a relatively low bias voltage (typically 400 V for an avalanche gain of 100) and achieves excellent noise characteristics. Currently, APDs are widely used in various fields of experimental physics and nuclear medicine. For example, APD-based modules have been proposed or tested for small animal imaging [4,5], while newly developed APD-arrays capable of achieving the ultimate sub-millimeter spatial resolution have been proposed [6,7].

Positron emission tomography (PET) has become one of the most efficient imaging techniques in detecting cancer as well as in diagnosing Alzheimer's in its early stages. In particular, PET combined with CT has proven a valuable multimodal imaging device revealing both functional and anatomic information. However, CT imaging suffers from limited soft-tissue contrast, with patients also subjected to a significant radiation dose that exceeds that received from the PET itself. Unlike CT, however, MRI offers several advantages such as good soft-tissue contrast and

* Corresponding author.
E-mail address: m4f2e7a8@asagi.waseda.jp (M. Yoshino).

0168-9002/$ - see front matter © 2011 Elsevier B.V. All rights reserved.
doi:10.1016/j.nima.2011.03.045

Table 1
Basic characteristics of BGO, LYSO, and Pr:LuAG scintillators.

	BGO	LYSO	Pr:LuAG
Density (g/cm^3)	7.13	7.10	6.73
Light yield (photons/MeV)	8200	25,000	20,000
Decay time (ns)	300	40	20
Peak wavelength (nm)	480	420	310

anatomical detail without additional radiation. Recently, there has been growing interest in using MRI-PET and various test systems have been proposed mainly for small animal research [8–10]. Unfortunately, traditional PET detectors based on photomultiplier tubes (PMT) cannot be used within the MRI high magnetic field. Conversely, the internal gain of the reverse-type APD produced by Hamamatsu is unaffected, even by the presence of a 7.9 T magnetic field [11], and hence applicable in simultaneous MRI-PET imaging [9,10].

There is also a wide-ranging choice of scintillators to be used in the PET scanner. Despite being the PET scintillator of choice for over two decades, bismuth germanate (BGO) is no longer used in modern PET scanners because of its low light output (15% of NaI(Tl)) and long scintillation decay time(300 ns) [12,13]. These disadvantages are overcome by the use of lutetium oxyorthosilicate (LSO) or lutetium-yttrium orthosilicate (LYSO), which is most popular at present. LYSO (or LSO) has a light output of 75% of NaI(Tl) and a scintillation decay time of around 40 ns, with a density comparable to that of BGO (7.1 g/cm^3) [14]. Alternatively, brand-new scintillators with higher light output and/or fast timing properties are being investigated for future application in a Time-Of-Flight PET scanner. Praseodymium (Pr)-doped $Lu_3Al_5O_{12}$ (Pr:LuAG) is one such scintillator characterized by a very fast decay time (20 ns; see Table 1) [15–17]. Although the light yield of Pr:LuAG is slightly smaller than that of LYSO, an excellent energy resolution of 4.8% (FWHM) at 662 keV was obtained with a thin $5\times5\times1$ mm^3 sample, as measured with a PMT (Hamamatsu H6531) [17].

Unfortunately, conventional APD is difficult to use as a photosensor coupled with the Pr:LuAG scintillator. This is because the light emission of Pr:LuAG is sharply concentrated at around 310 nm and most silicon detectors, like APDs, are less sensitive in the UV range. For example, it is known that QE of the Hamamatsu reverse-type APD, S8664 series, is less than 5% as shown in Fig. 1 (blue dashed line). This motivated us to newly develop UV-enhanced APD-arrays specifically matching Pr:LuAG scintillators, that achieve an excellent QE of 55%, as measured at 310 nm. The initial performance of the newly developed APD-arrays will be presented below in a simple PET device consisting of an APD-array optically coupled with a Pr:LuAG scintillator matrix.

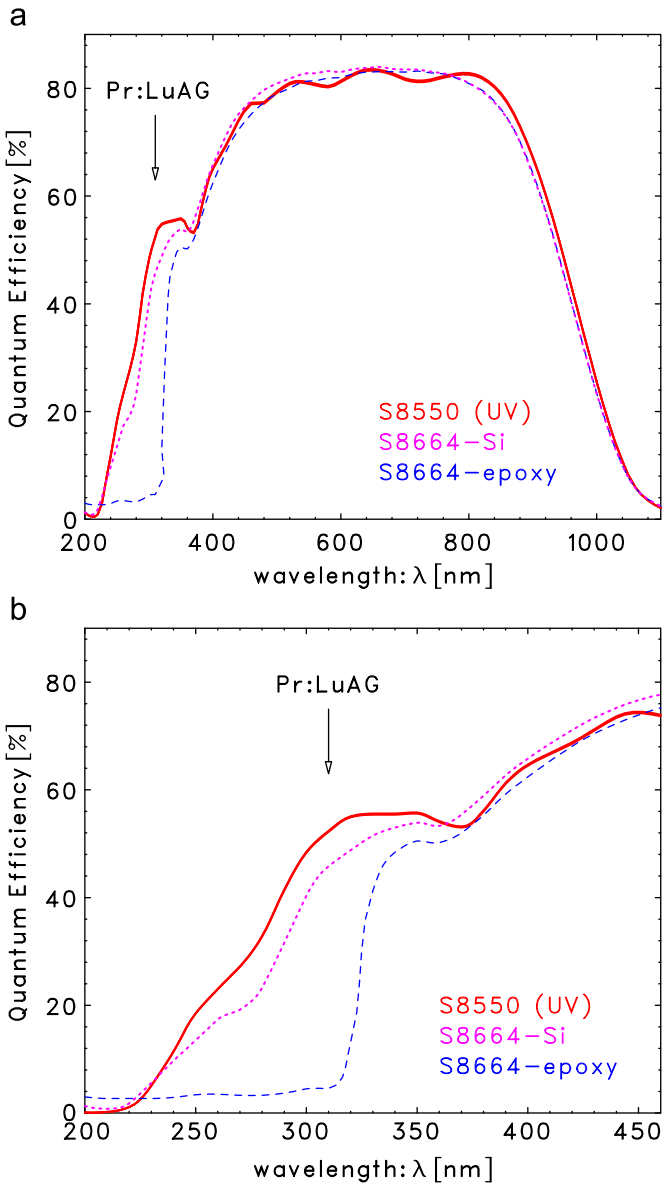

Fig. 1. Comparison of QEs for various APD types. *Top*: Overall response between 200 and 1100 nm and *bottom*: close up of UV region from 200 to 460 nm. Blue dashed line: Conventional reverse-type APD with epoxy resin window (Hamamatsu S8664 series), magenta dotted line: conventional reverse-type APD but with silicon resin window (Hamamatsu S8664 series), and UV-enhanced APD with silicon resin developed in this paper window (Hamamatsu S8550 series). Peak emission wavelength of Pr:LuAG is also represented. (For interpretation of the references to color in this figure legend, the reader is referred to the web version of this article.)

2. UV-enhanced APD-array

The APDs described here (Hamamatsu S8550-0001(X), -0002(X)) were developed based on the technology of the S8664 APD series (reverse-type). To enhance the UV sensitivity, we initially made a test sample of a monolithic 2×2 mm^2 APD, the entrance window of which was switched from conventional epoxy resin to silicon resin, while the silicon wafer itself remained unchanged. Even with this simple change, QE at 310 nm significantly improved to 46% as shown in Fig. 1 (magenta dotted line). Preliminary tests using the monolithic APD (2×2 mm^2 in size) with a Si-resin window coupled with a Pr:LuAG scintillator of $2.15\times2.15\times10$ mm^3 in size, have been reported [18]. Next we optimized the surface of the silicon wafer to maximize the QE at around 310 nm. Consequently, an excellent QE of 55% was obtained as shown in Fig. 1 (red solid line). Furthermore, as an application for the PET scanner, we succeeded, for the first time, in developing two types of large area, UV-enhanced APD-arrays (TYP1 and TYP2).

Table 2 lists the design parameters, dark noise and gain characteristic of each APD device. Both APD-arrays are embedded in a ceramic package with identical configuration and are 31.8×31.8 mm^2 in size. Photographs of the TYP1 (*left*) and TYP2 (*right*) APD-arrays developed here are shown in Fig. 2. The TYP1 APD-array has an 8×8 pixel structure with an active area of 3.05×3.05 mm^2 per pixel and a 0.25 mm gap between them. The TYP2 APD-array has a 12×12 pixel structure with an active area

of 2.05×2.05 mm^2 per pixel and a 0.25 mm gap between them. Our APD-arrays allow stable operations at a gain of around 100, with extremely low dark noise (less than 1.81 nA/pixel; Table 2) for each pixel, even at room temperature ($+25$ °C). An avalanche gain of 100 is also achieved with bias voltages of 388 and 382 V, respectively. The gain uniformity and dark current distributions of TYP1 and TYP2 APD-arrays, operated at a gain of 100 are shown in Figs. 3 and 4. Note the excellent uniformity of the avalanche gain (*left*) with low leakage current distributions (*right*). The gain fluctuation is only $\pm 8\%$ over the APD device. Note that UV-enhanced APD-arrays are made of a monolithic Si-wafer (of 6 in. diameter) and gain gradient is mostly due to the uniformity of Si-wafer itself, as show in Figs. 3 and 4.

3. Pr:LuAG scintillator

To date, various attempts have been made to establish the mass production of Pr:LuAG single crystals for general application to radiation detectors [13]. Two-inch diameter Pr:LuAG have been commercially available, but to further improve Pr:LuAG on scintillator markets, the size and quality of Pr:LuAG single crystal must be increased to enhance production efficiency and reduce costs. For this purpose, we made a large Pr:LuAG single crystal of diameter 92 mm, which was grown using the Czochralski (Cz) method [13]. Especially thanks to various optimizations of growth conditions, the quality and performance of the Pr:LuAG scintillator were dramatically improved. This large crystal was cut into a $10 \times 10 \times 10$ mm^3 cube shape with a mechanically polished surface.

Table 2
Basic characteristics of UV-enhanced APD-arrays.

	TYP1	TYP2
Matrix array	8×8	12×12
Pixel size (mm^2)	3.05×3.05	2.05×2.05
Pixel gap (mm)	0.25	0.25
Dark current (M=100): I_D (nA)	0.57–1.81	0.28–1.13
Break-down voltage: V_{brk} (V)	413	408
Operation bias: $V_{M=100}$ (V)	387.7	382.2
Capacitance: C_{det} (pF)	23–26	10–12

All parameters are measured at $+25$ °C.

Before testing with a UV-enhanced APD-array, we initially evaluated the Pr:LuAG scintillator itself with a PMT (Hamamatsu R3998) employing a super-bialkali photocathode, by irradiating 662 keV gamma-rays from ^{137}Cs. Each of the Pr:LuAG pieces was coated with the $BaSO_4$ based reflector and optical glues were used for the optical coupling between the PMT and Pr:LuAG scintillator. The output signal from the PMT was fed into a preamplifier (ClearPulse 506E) and a shaping amplifier (ORTEC 570; shaping time 3 μs), then finally digitized with a multichannel analyzer (Amptek MCA8000A). The operation bias of the PMT was set to 1000 V.

Fig. 5 (red solid line) presents the energy spectrum taken with the sample from 92 mm ∅ crystal as described above, measured at $+25$ °C. The energy spectrum taken with conventional Pr:LuAG (blue dashed line; taken from old 50 mm ∅ crystal) as well as the BGO of equivalent size (black dotted line; $10 \times 10 \times 10$ mm^3) are also given in the figure. Note an excellent energy resolution of 4.2% (FWHM) measured with the new Pr:LuAG crystal, compared with conventional Pr:LuAG (4.8% FWHM) and BGO sample (9.3% FWHM) under the same measurement conditions. Indeed, this is the best energy resolution obtained with the Pr:LuAG scintillator ever reported in literature. The light yield of the sample from 92 mm ∅ Pr:LuAG was about 30% larger than that of conventional 50 mm ∅ Pr:LuAG.

4. Fabrication and testing of the APD-Pr:LuAG detector

Finally, a prototype gamma-ray camera, consisting of a UV-enhanced APD-array optically coupled with a Pr:LuAG matrix, was fabricated. Fig. 6 shows a picture of the 12×12 Pr:LuAG

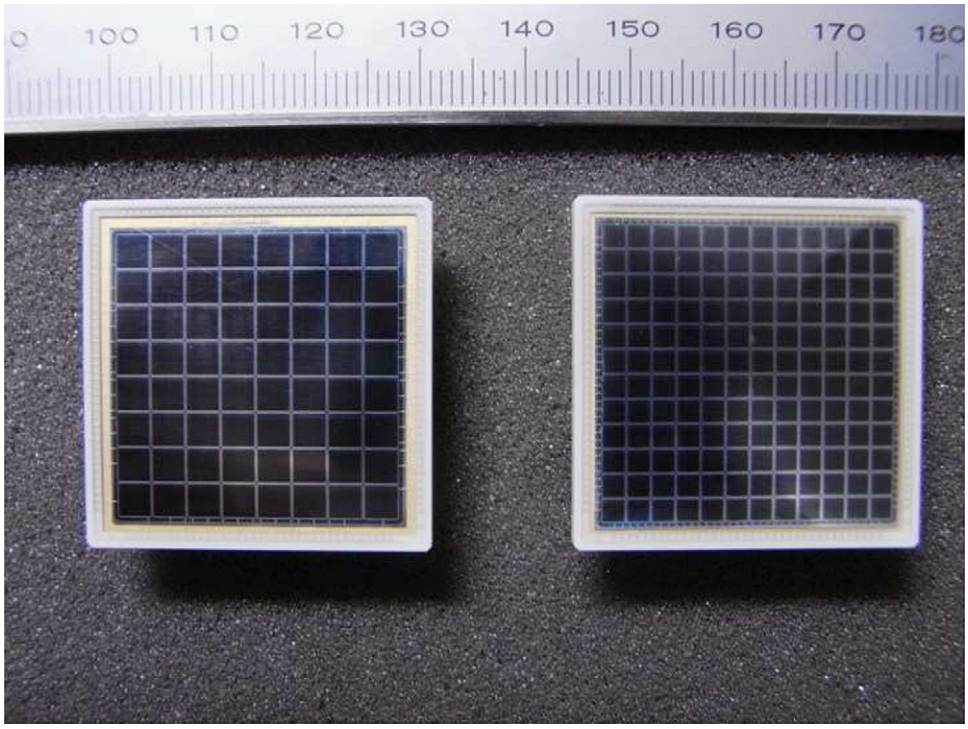

Fig. 2. A picture of the UV-enhanced APD-arrays developed in this paper (*left*: TYP1 8×8 array and *right*: TYP2 12×12 array).

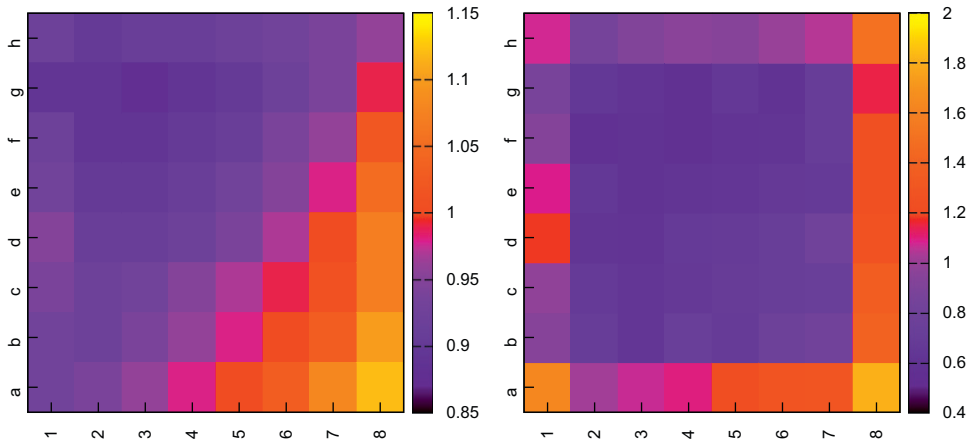

Fig. 3. Gain uniformity (*left*) and dark current distribution (*right*) of the UV-enhanced APD-array TYP1 operated at a gain 100.

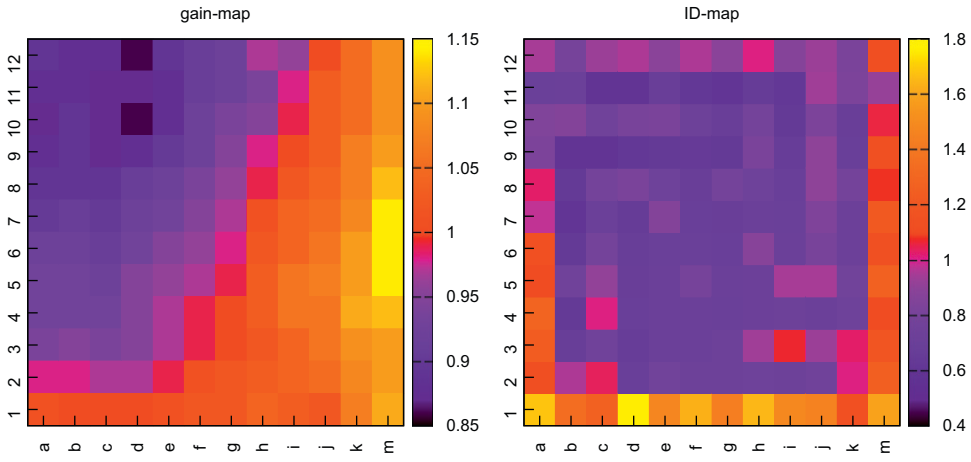

Fig. 4. Gain uniformity (*left*) and dark current distribution (*right*) of the UV-enhanced APD-array TYP2 operated at a gain 100.

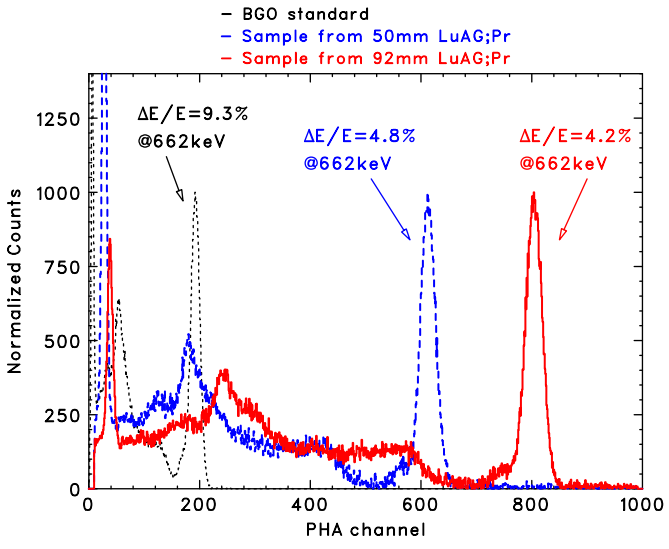

Fig. 5. Background subtracted energy spectra of ^{137}Cs measured with the newly fabricated Pr:LuAG sample from 92 mm ∅ crystal (red solid line), conventional Pr:LuAG sample from 50 mm ∅ crystal (blue dashed line) and BGO scintillator (black dotted line). Measured scintillator samples are all $10\times10\times10$ mm^3 in size. (For interpretation of the references to color in this figure legend, the reader is referred to the web version of this article.)

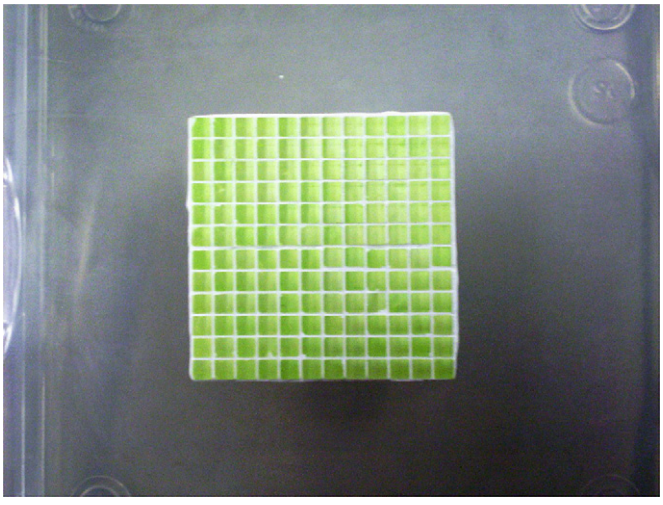

Fig. 6. A picture of the 12×12 Pr:LuAG scintillator matrix to be coupled with the TYP2 UV-enhanced APD-array (Fig. 2: *right*).

matrix for the TYP2 APD array, where each pixel is $2\times2\times10$ mm^3 in size and divided with a reflective $BaSO_4$ layer of 0.2 mm thickness. Similarly, the pixel size of each Pr:LuAG is $3\times3\times10$ mm^3 for the TYP1 APD-array. The APD signals were

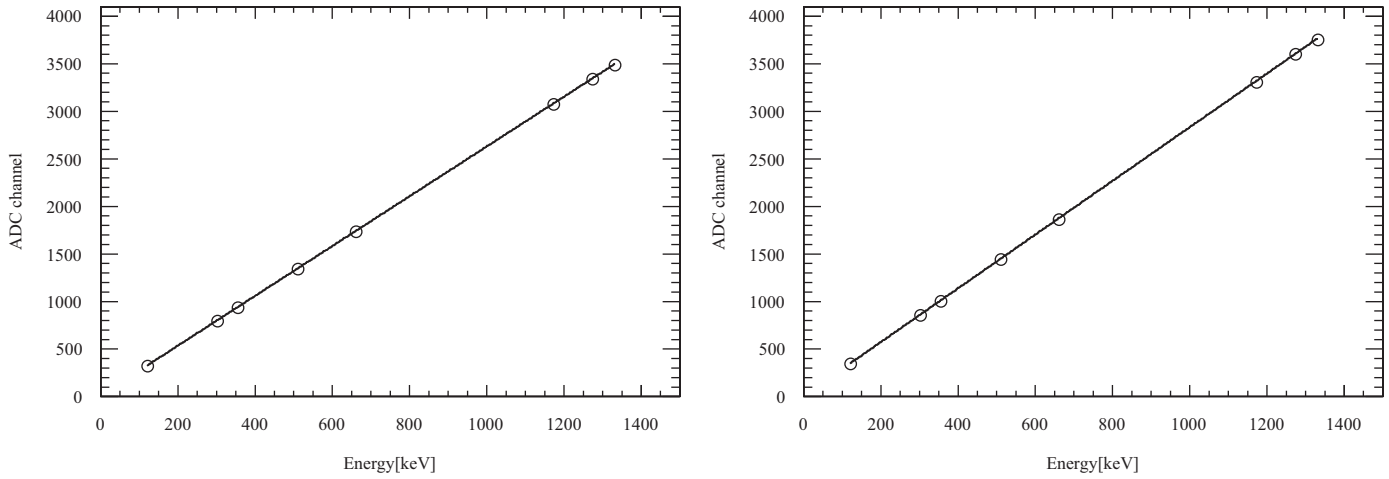

Fig. 7. Linearity of the MCA channel versus the energy of the incident radiation in TYP1 (*left*) and TYP2 (*right*) gamma-ray detectors. Circles and line represent the actual measured value and fitting function, respectively.

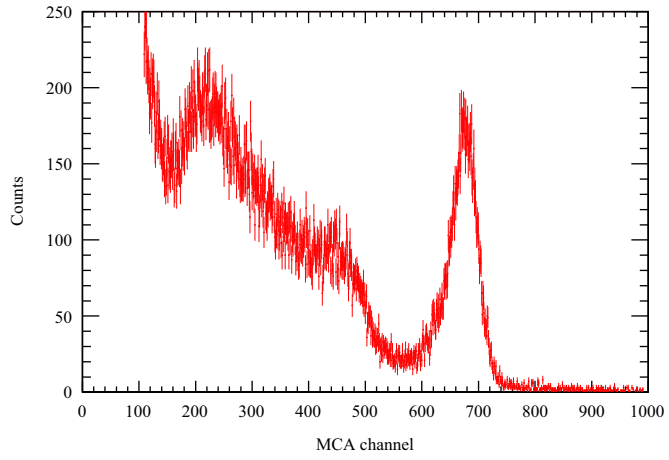

Fig. 8. An example of a 662 keV gamma-ray spectrum measured with the 8×8 gamma-ray detector consisting of the TYP1 APD-array and Pr:LuAG scintillator matrix.

fed into a preamplifier (ClearPulse 581 K), a shaping-amplifier (ORTEC 570; shaping time 2 μs), and finally digitized with a multichannel analyzer (Amptek MCA8000A). We operated TYP1 and TYP2 APD-arrays under bias voltages of 388 and 390 V, respectively. All the data were taken at $+25$ °C.

We first characterized the linearity of the APD-Pr:LuAG detector developed in this paper. Various gamma-ray sources, ^{22}Na, ^{57}Co, ^{60}Co, ^{133}Ba and ^{137}Cs were used for this calibration. Fig. 7 shows the relation between the output signal (the pulse height of the ADC channel) and incident gamma-ray energy. Note an excellent linearity of only 0.27% deviation for the TYP1 detector from the best-fit linear function (0.33% deviation for the TYP2 detector).

Fig. 8 shows an example of an energy spectrum obtained with a single pixel in the TYP1 APD-Pr:LuAG matrix for the ^{137}Cs source. The energy resolution of the 662 keV gamma-rays is 6.4% (FWHM). Figs. 9 and 10 show the distribution maps of the pulse height ADC channels (*left*), an energy resolution of 662 keV gamma-rays (in FWHM; *center*), and the light yield uniformity of the 8×8 and 12×12 Pr:LuAG scintillator matrix itself (*right*), namely, the pulse height of the γ-ray signal divided by the APD gain (arbitrary unit). In summary, the energy resolutions of the 662 keV photoelectric peak measured with the TYP1 and TYP2 gamma-ray detector are 7.0 ± 0.2 and 9.0 ± 0.6%, respectively. The variation of the signal amplitude (due to inhomogeneities of the APD gain and Pr:LuAG light yield) was only ±3.7% among 8×8 pixels for the TYP1 APD array (±7.7% among 12×12 pixels for the TYP2 APD array).

Finally we report the coincidence timing resolution of Pr:LuAG crystals with UV-enhanced APD-array readout in reference to a Pr:LuAG scintillator ($10\times10\times10$ mm^3) coupled to a PMT (Hamamatsu R3998). While the output signal of the reference detector was directly fed into the constant fraction discriminator (CFD: ORTEC 935), the output of the APD array was fed into a preamplifier (ClearPulse 581 K), a fast filter-amplifier (ClearPulse 4467A: shaping time 20 ns), and CFD (ORTEC 935). The outputs of the CFD were sent to a time-to-amplitude converter (TAC: ORTEC 567) with a maximum range of 500 ns, then finally digitized by MCA (Amptek 8000A) with 16,384 ch resolution (31 ps/ch). The timing resolution tests were carried out for 511 keV annihilation quanta from a ^{22}Na source. In this measurement the APD-array were operated under a bias voltage of 390 V, corresponding to an avalanche gain of $\simeq100$. Fig. 11 shows the coincidence time spectrum after walk correction and the precise selection of the energy windows around the full energy peak. A measured time resolution of 4.0 ± 0.1 ns (FWHM) was obtained.

5. Conclusion

In this paper, we overviewed the performance of newly developed large-area, UV-enhanced APD-arrays. The latter are specifically designed to be capable of coupling with the Pr:LuAG scintillator. An excellent QE of 55% was obtained at a peak scintillation wavelength of Pr:LuAG of around 310 nm. We also obtained effective gain uniformities of less than 5.1 and 7.9% and low dark current noise of below 1.9 and 1.8 nA in TYP1 and TYP2 APD-array at gain 100, respectively. Next, we fabricated new Pr:LuAG samples from 92 mm ∅ crystal and obtained 4.2% (FWHM) at 662 keV, as measured with a PMT employing the super-bialkali cathode. This is the best energy resolution ever reported, taken with the $10\times10\times10$ mm^3 Pr:LuAG scintillator. When UV-enhanced APD-arrays were coupled with the Pr:LuAG scintillator matrix, a good linearity with only 0.27% and 0.33% deviation from the best-fit linear function were measured, respectively, for TYP1 and TYP2 detectors. An excellent energy resolution of $7.0\%\pm0.2\%$ was obtained with the TYP1 detector as compared to $9.0\%\pm0.6\%$ with the TYP2 detector, respectively. Pulse height uniformity of less than ±3.7% and 7.7% with

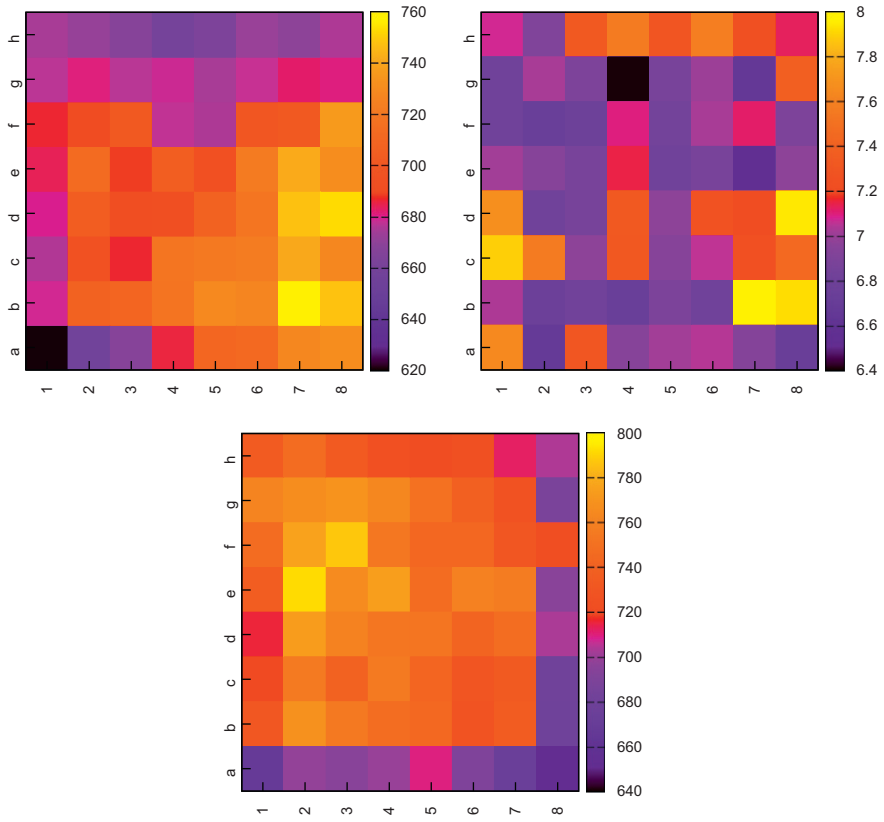

Fig. 9. From *top* to *bottom*: the pulse height uniformity (in the ADC channel), energy resolution (FWHM in %), and light yield of the Pr:LuAG scintillator (arbitrary unit) measured with an 8×8 gamma-ray detector consisting of a TYP1 APD-array coupled with a Pr:LuAG scintillator matrix, irradiated by a ^{137}Cs source.

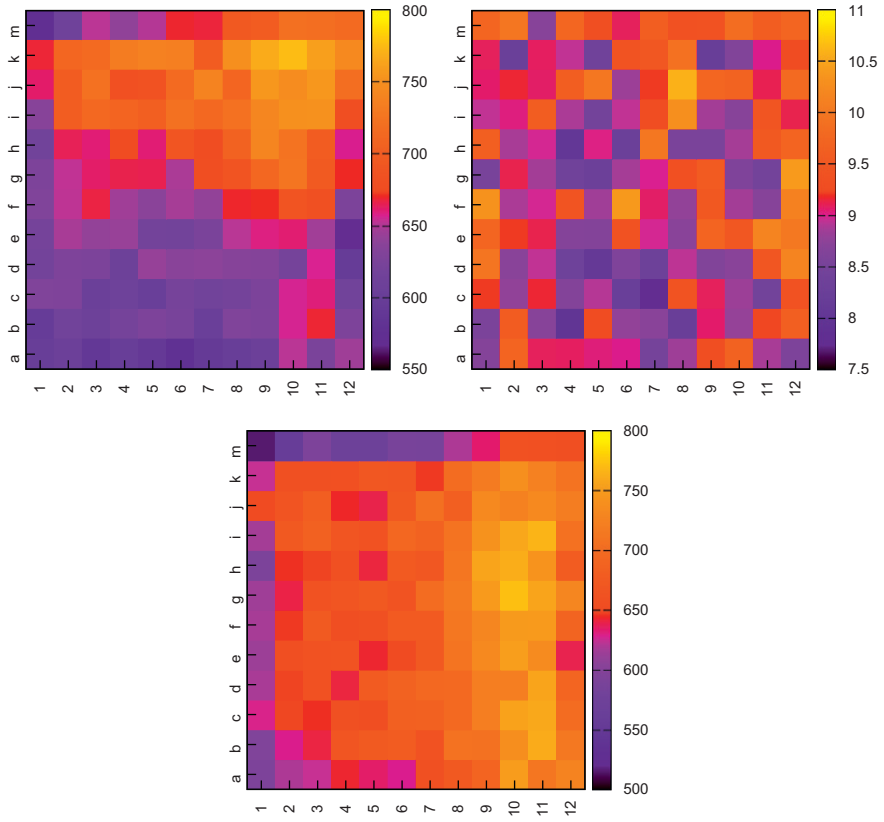

Fig. 10. From *top* to *bottom*: the pulse height uniformity (in the ADC channel), energy resolution (FWHM in %), and light yield of the Pr:LuAG scintillator (arbitrary unit) measured with a 12×12 gamma-ray detector consisting of a TYP2 APD-array coupled with the Pr:LuAG scintillator matrix, irradiated by the ^{137}Cs source.

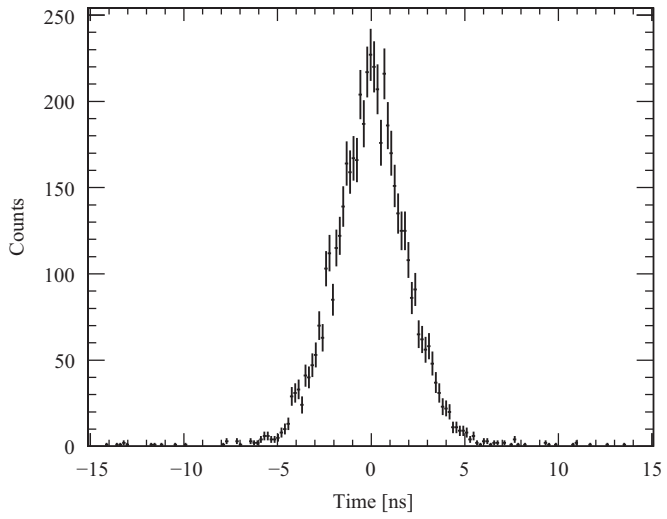

Fig. 11. A timing spectrum measured with the annihilation quanta from a ^{22}Na source.

the TYP1 and TYP2 detector were also reported. We obtained a coincidence timing resolution of 4.0 ± 0.1 ns for these gamma-ray detectors for 511 keV gamma-rays from ^{22}Na sources. These results suggest that the UV-enhanced APD-arrays are promising devices for future APD-based PET detectors.

Acknowledgments

We deeply appreciate the insightful comments and suggestions of the anonymous referee to improve the manuscript.

References

[1] T. Ikagawa, et al., Nucl. Instr. and Meth. A 515 (2003) 671.
[2] T. Ikagawa, et al., Nucl. Instr. and Meth. A 538 (2005) 640.
[3] J. Kataoka, et al., Nucl. Instr. and Meth. A 541 (2005) 398.
[4] M. Bergeron, et al., IEEE Trans. Nucl. Sci. NS-56 (1) (2009) 10.
[5] D.P. McElroy, et al., IEEE Trans. Nucl. Sci. NS-52 (1) (2005) 199.
[6] J. Kataoka, et al., Nucl. Instr. and Meth. A 604 (2009) 323.
[7] J. Kataoka, et al., IEEE Trans. Nucl. Sci. NS-57 (5) (2010) 2448.
[8] H. Peng, et al., Nucl. Instr. and Meth. A 612 (2010) 412.
[9] C. Woody, et al., Nucl. Instr. and Meth. A 571 (2007) 102.
[10] B.J. Pichler, et al., J. Nucl. Med. 47 (4) (2006) 639.
[11] J. Marler, et al., Nucl. Instr. and Meth. A 449 (2000) 311.
[12] L. Eriksson, et al., Nucl. Instr. and Meth. A 525 (2004) 242.
[13] K. Kamada, et al., IEEE Trans. Nuclear Science Conference Record, N25-98.
[14] G. Ioannis, et al., Nucl. Instr. and Meth. A 569 (2006) 201.
[15] H. Ogino, et al., J. Cryst. Growth 292 (2006) 239.
[16] L. Swiderski, et al., IEEE Trans. Sci. NS-56 (2009) 2499.
[17] W. Droxdowski, et al., IEEE Trans. Nucl. Sci. NS-55 (4) (2008) 2420.
[18] K. Kamada, et al., IEEE Trans. Nucl. Sci. Conference Record, N28-2.